Z. Kristallogr. **222** (2007) 601–604 / **DOI** 10.1524/zkri.2007.222.11.601

Grazing exit small angle X-ray scattering on grain formation in polycrystalline metal films

Wei Zhang[I] and Ian K. Robinson*,[II]

[I] Department of Materials Science and Engineering, University of Illinois at Urbana-Champaign, Urbana, IL 61801, USA
[II] London Centre for Nanotechnology, University College, Gower St, London, WC1E 6BT, United Kingdom and
Diamond Light Source, Harwell Science and Innovation Campus, Didcot, OX11 0DE, United Kingdom

Received March 13, 2007; accepted August 14, 2007

Grain size distribution / Metal thin films / X-ray diffraction / GESAXS / Nanostructures

Abstract. We recently proposed a new grazing exit geometry for measuring the small-angle scattering from thin film materials, which we call GESAXS, to contrast with the successful grazing incidence version, GISAXS. The technique is particularly useful for probing nanostructured thin film materials, especially when the coherence properties of the beam are employed. Here we demonstrate the application of GESAXS to evaporated metal films, prepared using an in-situ diffraction chamber, to investigate how their structure evolves upon annealing. Contrasting behavior is seen for Au, which preserves a roughly exponential distribution of domain sizes, and Fe for which the size distribution narrows by an Ostwald ripening process.

1. Introduction

The structure of thin film materials determines a wide range of properties that are used in a wide range of applications, for example coatings used in biological sensors or electrodes in display technology [1]. The structure of thicker deposits is frequently determined by the outcome of the first layers, which can often be very different from the bulk. For metals, annealing at a strategic stage of deposition can lead to an interesting range of subsequent structures through templating. The critical length scale for these structures is a few nanometers, for which the behavior upon annealing is significantly different from the bulk. Pattern formation is determined by the competing processes of surface and bulk diffusion, surface tension and dewetting from the substrate.

X-ray diffraction is the traditional method of examining these structures because it penetrates the entire sample and can be used in-situ during growth. New third-generation synchrotron sources have sufficient flux that very thin samples can be routinely examined, even when the crystalline order is relatively poor. The very high brightness leads to improved coherence, which can be exploited for direct imaging of individual grains [2] or probing dynamics through 'speckle' interference methods [3].

There are a number of important ways of improving the sensitivity for thin film samples using grazing incidence and exit conditions on the X-ray beams. This also takes advantage of the high brightness of the latest sources, where both the divergence and the footprint of the beam on the sample must be minimized. We recently proposed a new grazing exit small-angle X-ray scattering (GESAXS) geometry for measuring thin films [4]. In contrast with the grazing incidence version, GISAXS, this uses a steeper incidence angle (above the critical angle) to ensure the whole sample depth is illuminated. This confines the footprint of the beam on the sample to a smaller region that allows the use of area detectors on the scattered beam. By analyzing the exit beam directions in the vicinity of the critical angle, GESAXS resolves contributions from different depths within the sample, hence is sensitive to layering. GESAXS is the preferred geometry for seeing the coherence effects also [4].

GISAXS and GESAXS methods inherently involve dynamical diffraction, so the intensity distributions and beam positions observed are modified by wave interference effects. It is not sufficient to apply the simple kinematic approximation that all parts of the sample scatter independently. Much work has been done to predict and exploit these dynamical effects [5]. Here we show that our GESAXS results can be explained by a combination of three physical processes: refraction and transmission (Fresnel coefficient) at the interfaces combined with single scattering from the sample.

2. GESAXS experiment

The experiments were performed at the undulator beamline 34-ID-C of the Advanced Photon Source using monochromatic radiation of 8.92 keV. Polycrystalline metal films of Au and Fe were investigated. The Au sample was a 1000 Å thin film deposited ex-situ by thermal evaporation at room temperature onto a piece of $15 \times 15\,\mathrm{mm}^2$ polished quartz substrate. During annealing, the sample was heated by a ceramic-enclosed graphite heater under

* Correspondence author (e-mail: i.robinson@uc.ac.uk)

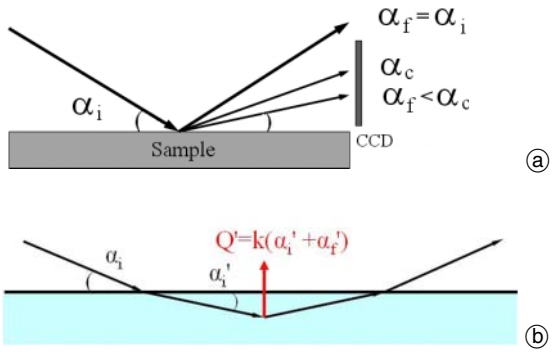

Fig. 1. (**a**) Sketch of the geometry used in the experiment. The out of plane direction is referred to as angle ϕ. (**b**) Schematic wave picture of the DWBA scattering processes involved with scattering from within the depth of the film. Both incident and exit waves undergo refraction, while kinematical scattering is assumed to take place within the film. In the GESAXS case shown in Fig. 1a, the incident angle α_i is large enough that its refraction is quite small; the depth sensitivity then arises from the variation of exit angle α_f.

the sample. Thermocouple wires welded onto the tantalum sample holder were used to measure the temperature of the sample.

The grazing exit geometry of the experiments is illustrated in Fig. 1. The samples were tilted forward to have an incident angle of typically 0.8 to 1.2 deg, two to three times of the critical angle α_c of the materials investigated. A CCD X-ray camera with a pixel size of 22.5 μm was placed on the detector arm of the diffractometer at about 2 m far from the sample to collect the scattered intensities in the grazing exit angular range $0 < \alpha_f < \alpha_c$.

2.1 Results for gold

Three general components are expected under these conditions: a specular beam, an off-specular ridge of intensity within the scattering plane due to the surface roughness and a diffuse scattering from the distribution of bulk grains taking a "triangle shape" [4]. However, in the case of a very flat sample, the off-specular ridge will be missing. Figure 2a is an example of the scattering intensity image from a 1000 Å thick gold film, before annealing, in which there is no off-specular ridge.

Since we expect the scattering from a polycrystalline sample to be weak, it can be calculated quasi-kinematically within the "distorted-wave Born approximation" (DWBA) shown in Fig. 1b. The scattered intensity is given by

$$I(\alpha_f, \phi) = I_{\mathrm{SAXS}}(\alpha_f, \phi) \times |T_i|^2 \times |T_f|^2 \tag{1}$$

where the details of the structure being probed are buried in the I_{SAXS} factor. The electric-field amplitude transmission functions for the incident and exit beam are given by the Fresnel coefficients [6, 7].

$$|T_f|^2 = \frac{4\alpha_f^2}{\left(\alpha_f' + \alpha_f\right)^2 + \alpha_f''^2}\,; \qquad |T_i|^2 = \frac{4\alpha_i^2}{\left(\alpha_i' + \alpha_i\right)^2 + \alpha_i''^2}\,. \tag{2}$$

The real (propagating) and imaginary (evanescent) parts of the complex angle of the exit beam inside the sample are given by

$$\alpha_f' = \sqrt{\frac{1}{2} \times \left(\sqrt{\left(\alpha_f^2 - 2\delta\right)^2 + 4\beta^2} + \left(\alpha_f^2 - 2\delta\right)\right)}\,; \qquad \alpha_f'' = \sqrt{\frac{1}{2} \times \left(\sqrt{\left(\alpha_f^2 - 2\delta\right)^2 + 4\beta^2} - \left(\alpha_f^2 - 2\delta\right)\right)} \tag{3}$$

where the complex refractive index of the material is given by $n = 1 - \delta + i\beta$. Since the incident angle is fixed, the transmission function $|T_i|^2$, real and imaginary angle inside the sample for the incident beam α_i', α_i'' are all constant during a given measurement. The unique feature of GESAXS is that $\alpha_i \gg \alpha_c$, so the incident beam is mostly real and illuminates the full depth of the sample.

$I_{\mathrm{SAXS}}(\alpha_f, \phi)$ is the lineshape function of the small angle scattering, which needs to account for the refraction effect in the out-of-plane direction. In the in-plane direction (q_y, or ϕ), there is a constant refraction effect on the scattering, so the lineshape function is only a function of ϕ. Figure 2c is the scattered signal along a horizontal slice across the middle of the "triangle" in Fig. 2a and the red line is a fit to the data with a "Lorentzian squared function" given by $I_{\text{in-plane}}(\phi) = \dfrac{C}{\left(\phi^2 + W^2\right)^2}$. For different exit angles α_f, the width of the function, W, was found to be the same, while the scale factor C was different.

Assuming the material of the film is isotropic and not strongly textured, the small angle scattering inside the sample will be symmetric in q_y and q_z, the directions parallel and perpendicular to the sample surface. Since q_y and q_z in the small-angle approximation are proportional to ϕ and $\alpha_i' + \alpha_f'$, the overall lineshape function within the sam-

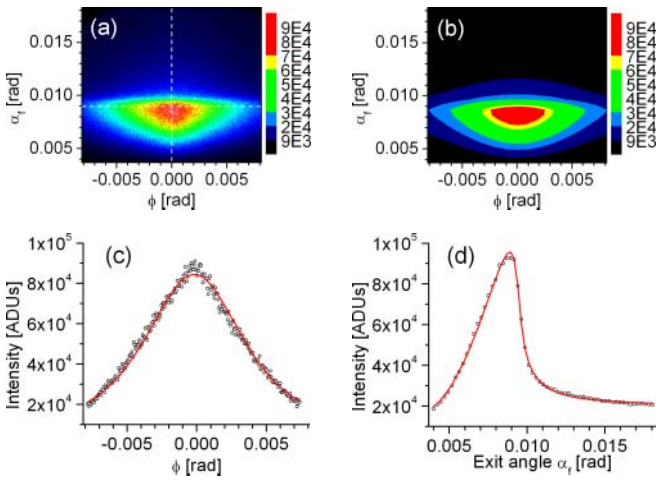

Fig. 2. (**a**) Measured GESAXS intensity as a function of ϕ and α_f from a gold film of 1000 Å as deposited, with an incident angle $\alpha_i = 0.0192$ rad (1.1 deg). (**b**) Two dimensional fitting of the intensity distribution in Fig. 2a by Eq. 5. (**c**) Intensity plot (circles) of white horizontal dashed line across Fig. 2a, as a function of ϕ with $\alpha_f = 0.0087$ rad, and the Lorentzian squared function fit (red line) to the data. (**d**) Intensity plot (circles) of the white vertical dashed line across Fig. 2a, as a function of α_f with $\phi = 0$, and the Lorentzian squared function fit (red line) where the exit-beam refraction effects are included.

ple will be given by

$$I_{\mathrm{SAXS}}(\alpha_f,\phi) = \frac{C'}{(q_{2D}^2+\Delta q^2)^2} = \frac{C'}{(q_z^2+q_y^2+\Delta q^2)^2} = \frac{C}{((\alpha_i'+\alpha_f')^2+\phi^2+W^2)^2} \quad (4)$$

so that outside the sample it will be

$$I(\alpha_f,\phi) = I_{\mathrm{SAXS}}(\alpha_f,\phi)\cdot|T_i|^2\cdot|T_f|^2 = \frac{C\cdot|T_i|^2}{((\alpha_i'+\alpha_f')^2+\phi^2+W^2)^2}\cdot\frac{4\alpha_f^2}{(\alpha_f'+\alpha_f)^2+\alpha_f''^2} \quad (5)$$

Figure 2d is the scattered intensity along a vertical slice across the middle of the "triangle" in Fig. 2a and the red line is the fitting with Eq. (5) with $\phi = 0$ and the same value of W as used to fit the horizontal slice. The fact that the data are consistent with a common value of W in both directions supports the assumption of an isotropic grain size distribution.

Having explained the shape in the two perpendicular diections we can construct the full intensity distribution on the detector in Fig. 2b with Eq. (5), using the same two dimensional scale for the intensity plot as in Fig. 2a.

From the analysis above, we know that the small angle scattering in the sample alone would give rise to a two-dimensional symmetric pattern centered at the incident direction, as in the transmission small-angle X-ray scattering (SAXS) geometry, which we illustrate schematically in Fig. 3a. For the grazing exit "reflection" GESAXS geometry, the scattered intensity forms a "triangle" shape pattern close to α_c, due to the combined effect of transmission and refraction. The electric field transmission function of the exit beam $|T_f|^2$ enhances the intensity near the critical angle $\alpha_f = \alpha_c$ to produce a "Yoneda" peak. The effect of the refraction on the lineshape function is illustrated in Fig. 3c: the lineshape function, I_{SAXS}, without the transmission function, would take the shape of "Lorentzian squared function" with respect to α_f', the exit angle inside

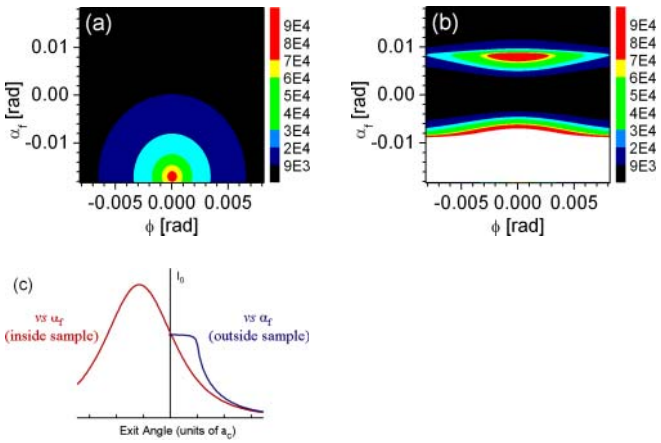

Fig. 3. (**a**) Simulated intensity distribution of just the small angle X-ray scattering (SAXS) in the transmission geometry at an incident angle $\alpha_i = 0.0192$ rad ($\alpha_i' = 0.0171$ rad). (**b**) Simulated intensity distribution of GESAXS with $\alpha_i = 0.0192$ rad. (**c**) Intensity of the SAXS lineshape function, I_{SAXS} with respect to the exit angle inside (red curve) and outside (blue curve) of the sample.

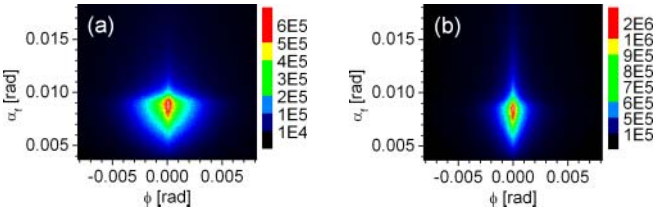

Fig. 4. Effect of annealing of the GESAXS patterns from a gold film (**a**) at 200 °C, (**b**) at 240 °C with $\alpha_i = 0.0192$ rad.

the sample, as the red curve shows. Due to the refraction effect, the range of angles (the flat plateau of the blue curve) outside the sample below the critical angle merge into a small range of the angles (close to the crossing point of y axis and the red curve) inside the sample, thus forming a "triangle" shape pattern close to α_c. The part of the signal below the sample "horizon" ($\alpha_f < 0$) is not measurable for the reflection geometry in our case.

The "Lorentzian squared" lineshape function we have found to fit the data in the intensity plot, is the Fourier transform of the exponential decay function in 3 dimensions: $FT_{3D}(\mathrm{e}^{-ar}) = \frac{1}{\pi}\frac{2a}{(a^2+q^2)^2}$. Since the primary contrast mechanism is the lower density associated with the grain boundaries of the polycrystalline film [4], the correlation function of the grain boundaries in the sample thus follows an exponential decay trend. We can therefore conclude that the grain size distribution is also exponential.

When the sample of a gold film of 1000 Å was annealed to 200 °C, the "triangle" diffuse scattering pattern was found to shrink in the out-of-plane direction to one with a smaller width, W. This is expected since the average grain size gets bigger during annealing and the average grain size follows an inverse relation with the width of the diffraction pattern. From the width of the horizontal intensity distribution, the average grain size is estimated to change from about 200 nm to a few microns. We note that the off-specular ridge feature (center of pattern above the "horizon") also tends to increase with annealing. This can be undestood from the consideration that the grain size exceeds the starting film thickness; when individual grains start to protrude from the surface of the film, the roughness will be greater.

2.2 Results for iron

The Fe film samples were deposited in-situ in the UHV chamber of beamline 34-ID-C at APS by an e-beam evaporator (with typically 18 W of power and 50 nA of beam current). A clean silicon wafer substrate was used without removing its thick grown oxide film. The starting pressure was 3×10^{-9} Torr and the deposition rate was 0.5 Å/sec. Grazing exit small angle scattering was performed during the deposition and annealing. The triangle shape "Yoneda" pattern began to show up at a film thickness of about 15 nm and the intensity continued to increase as more material was deposited. At the same time, fringes coming from the interference between the signals from top and bottom of the film were observed above the critical angle $\alpha_f = \alpha_c$. From the fringes spacing, the film thickness can be calculated.

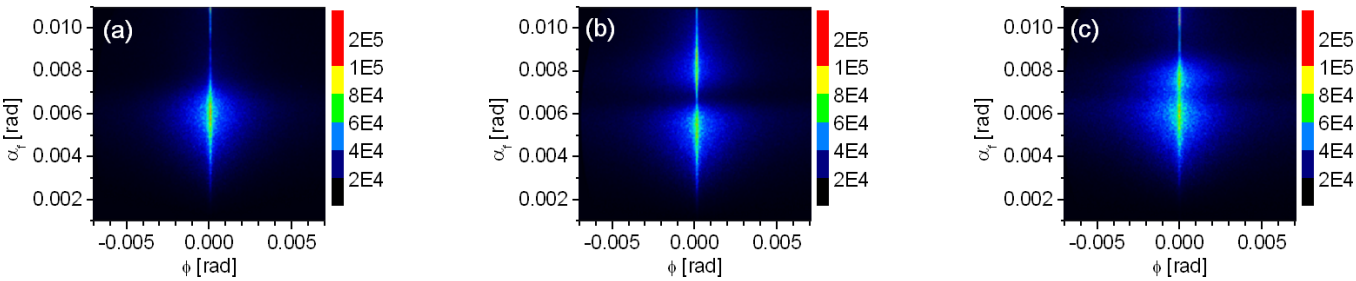

Fig. 5. GESAXS patterns from a Fe film e-beam evaporated onto a silicon sample, measured during *in-situ* deposition with $\alpha_i = 0.014$ rad (0.8 deg). From the vertical fringe spacing, the Fe film thicknesses for (**b**) & (**c**) were estimated to be 460 Å ($\Delta q_z \approx 0.0137$ Å^{-1}) and 590 Å ($\Delta q_z \approx 0.0107$ Å^{-1}).

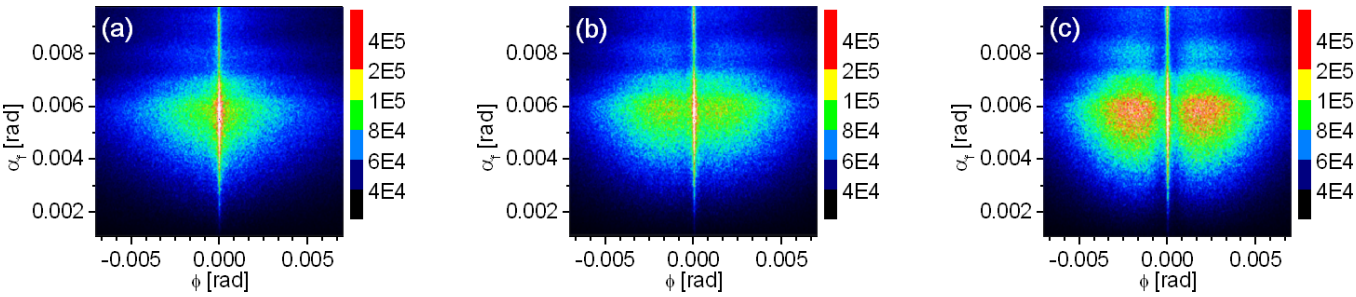

Fig. 6. GESAXS patterns of a Fe thin film on silicon with $\alpha_i = 0.014$ rad, the images were acquired at $t = 0$, $t = 15$ min, $t = 45$ min from the time the sample temperature was raised to 250 °C.

Measurements of another Fe film is shown in Fig. 6, after evaporation for 13 mins (with 18 W of power and 50 nA of beam current). The film thickness was calculated from the vertical fringe spacing to be 940 Å ($\Delta q_z \approx 0.0067$ Å). When the sample was annealed at 250 °C for about 15 mins, two side peaks were seen, which suggest a preferred correlation length (grain size) had appeared in the film. As the time-dependence in Fig. 6 shows, the intensity of the side peaks increased as the annealing went on. The intensity distribution of the side peaks is seen to become narrower in time suggesting the grain size distribution is also narrowing as would take place in an Ostwald ripening process [1].

The vertical fringe distribution remains approximately unchanged, suggesting the film integrity is not changing while the out-of-plane grain size distribution is narrowing. This suggests a columnar grain morphology with a well-defined thickness [1]. There is an increase in the intensity of the off-specular ridge, suggesting a small increase of surface roughness during the anneal, just as was found for the gold films.

3. Conclusion

Morphological changes have been observed in thin metal films of gold and iron during deposition and subsequent annealing in UHV. In the case of gold, no preferred size appears and the distribution of grain sizes remains approximately exponential after annealing, within the range of thicknesses, temperature and time investigated. Some roughening of the film was evident from the appearance of a non-specular ridge of intensity.

In the case of iron films, qualitatively different behaviour was observed. Thinner films of less dense material allowed the thickness oscillations to be recorded in the in-plane direction. Upon annealing, the out-of-plane grain-size distribution became narrower around a preferred size. This evolution took place without the film thickness changing.

The quantitative fitting to the in-plane and out-of plane lineshapes means we have gained a better understanding of the sequence of refraction and scattering processes associated with the GESAXS geometry.

Acknowledgments. This work was partially supported by EPSRC grant EP/D052939/1 (IKR). The 34-ID-C beamline facility at the Advanced Photon Source (APS) is supported by the U.S. DOE under Award No. DEFG02-91ER45439, through the Frederick Seitz Materials Research Laboratory at the University of Illinois at Urbana-Champaign, the Oak Ridge National Laboratory (U.S. DOE contract DE-AC05-00OR22725 with UT-Battelle LLC), the National Institute of Standards and Technology (U.S. Department of Commerce) and UOP LLC. The APS is supported by the U.S. DOE, Basic Energy Sciences, Office of Science under contract No. W-31-109-ENG-38.

References

[1] Thompson, C. V.: Structure evolution during processing of polycrystalline films. Ann. Rev. Mater. Sci. **30** (2000) 159–190.
[2] Robinson, I. K.; Miao, J. W.: Three-Dimensional Coherent X-ray Diffraction Microscopy. MRS Bulletin. **29** (2004) 177–181
[3] Malik, A.; Sandy, A. R.; Lurio, L. B.; Stephenson, G. B.; Mochrie, S. G. J.; McNulty, I.; Sutton, M.: Coherent X-ray Study of Fluctuations during Domain Coarsening. Phys. Rev. Lett. **81** (1998) 5832–5835.
[4] Pfeiffer, F.; Zhang, W.; Robinson, I. K.: Coherent Grazing Exit X-ray Scattering Geometry for Probing the Structure of Thin Films. Appl. Phys. Lett. **84** (2004) 1847–1849.
[5] Danis, S.; Holy, V.: Diffuse X-ray Scattering from GaN/SiC (0001) Thin Films. Z. Kristallogr. Suppl. **23** (2006) 141–146.
[6] Als-Nielsen, J.; McMorrow, D.: Elements of Modern X-ray Physics. Wiley, 2001.
[7] Born, M.; Wolf, E.: Principles of Optics. Pergamon Press, 1959.